# Proton Assisted Recoupling at High Spinning Frequencies

**Józef R. Lewandowski[†,§], Gaël De Paëpe[†,**], Matthew T. Eddy[†], Jochem Struppe[‡], Werner Maas[‡],** and **Robert G. Griffin[†,*]**

[†]Department of Chemistry and Francis Bitter Magnet Laboratory, Massachusetts Institute of Technology, Cambridge, Massachusetts 02139

[‡]Bruker BioSpin Corporation, Billerica, Massachusetts 01821

## Abstract

We demonstrate the successful application of $^{13}C$-$^{13}C$ proton assisted recoupling (PAR) on [U-$^{13}C$,$^{15}N$] N-$f$-MLF-OH and [U-$^{13}C$,$^{15}N$] protein GB1 at high magic angle spinning (MAS) frequencies ($\omega_r/2\pi$=65 kHz). Specifically, by combining PAR mixing with low power heteronuclear decoupling ($\omega_{1H}/2\pi\sim$16 kHz) and high spinning frequencies, we obtain high resolution 2D spectra displaying long range $^{13}C$-$^{13}C$ contacts from which distances can be extracted. These experiments therefore demonstrate the possibility of performing high resolution structural studies in the limit of high spinning frequency and low power $^1H$ decoupling, a regime which optimizes resolution of protein samples and preserves their integrity.

### Keywords

solid-state NMR; MAS; protein; low power decoupling

## Introduction

Over the past two decades the development and refinement of magic angle spinning (MAS) [1,2] NMR methods to perform dipolar recoupling[3] have established approaches to perform spectral assignments, measure distances and torsion angles, and therefore established the foundation for *de novo* protein structure determination with solid state NMR.[4–23] These methods are most relevant to several classes of important biological systems – specifically, nanocrystals, amyloid fibrils, and membrane proteins[24–2828]—that are inaccessible via other techniques. In addition, advances in instrumentation have contributed to the expansion of the repertoire of techniques available as structural tools. One such direction, pioneered by Samoson and coworkers, is the extension of MAS NMR spinning frequencies to the range of 50–70 kHz.[29,30] Access to MAS frequencies in this regime, which are larger than the size of $^1H$-$^1H$ dipolar couplings, has stimulated interest in the possibility of introducing a $^1H$ dimension into multidimensional MAS spectra, for example in direct detection experiments. [29,31–35] Concurrently, each new spinning frequency regime has required the development

---

[*]To whom correspondence should be addressed. Email: rgg@mit.edu.
[§]Current address: Université de Lyon, CNRS/ ENS Lyon/ UCB-Lyon 1, Centre RMN à Très Hauts Champs, 5 rue de la Doua, 69100 Villeurbanne, France
[**]Current address: Laboratoire de Chimie Inorganique et Biologique, UMR-E3 (CEA/UJF), CEA/DSM/INAC - 38054 Grenoble - France

of new or modified methodologies in order to optimize the resolution and sensitivity of NMR experiments. For instance, the capability of performing experiments at ($\omega_r/2\pi = 20$–35 kHz) led to the development of a number of new tools applicable at high magnetic fields ($B_0 > 15T$), that promise to be valuable for protein assignments and structural studies. [19,20,22,23,36] Two examples are cosine modulated rotary resonance (CMRR) and a version of RFDR[36] that do not require ^{1}H decoupling during mixing. Both of these approaches are less demanding of the power handling capabilities of the probe and preserve the integrity of the sample, and are therefore useful for ^{13}C resonance assignments and distance measurements in proteins at high $\omega_r/2\pi$. Furthermore, since CMRR it is a double quantum (DQ) experiment, the cross peaks are alternately negative and positive and provide data for unambiguous assignments[22]. In another advance we demonstrated new second order recoupling techniques based on the third spin assisted recoupling (TSAR) mechanism to constrain distances up to 5–7 Å in uniformly ^{13}C and ^{15}N labeled systems. In particular, in heteronuclear and homonuclear cases we employ proton assisted insensitive nuclei cross polarization (PAIN-CP)[20] and proton assisted recoupling (PAR)[23] experiments, respectively, which were subsequently used to calculate a *de novo* 3D protein structure.[37]

There have been a few reports of experiments at spinning frequencies >30 kHz; among them, Ernst and coworkers used low power ^{1}H decoupling (i.e. the ^{1}H rf field strength applied is smaller than the spinning frequency),[38] and performed [13]C-^{13}C correlation experiments on proteins in the >40 kHz spinning frequency regime.[39,40] However, the repertoire of SSNMR methods that function at $\omega_r/2\pi > 40$ kHz remains limited [16,41–43]and there is an especially notable paucity of techniques for measuring long distances. Thus, this is a regime that is ripe with opportunities for methodological developments.

In this manuscript we demonstrate that the homonuclear proton assisted recoupling (PAR)[23,44] pulse sequence can be successfully applied at $\omega_r/2\pi \sim 65$ kHz to uniformly ^{13}C and ^{15}N labeled proteins. The PAR technique, which relies on the TSAR[20,23] mechanism, is discussed in detail elsewhere for spinning frequencies $\omega_r/2\pi < 30$ kHz. Here we show that, despite the fact that the technique relies on a second order recoupling mechanism, it can still be used to observe long distance [13]C-^{13}C contacts with mixing times on the order of tens of milliseconds at $\omega_r/2\pi = 65$ kHz. It therefore provides an approach to provide the data necessary for protein structure determinations at high magnetic fields and spinning frequencies.

## Experimental Section

### Sample preparation

**Preparation of [U-^{13}C,^{15}N]-N-*f*-MLF-OH**—N-*f*-MLF-OH peptide was obtained by solid phase peptide synthesis (CS Bio Inc., Menlo Park, CA). The peptide was prepared with uniformly ^{13}C and ^{15}N labeled amino acids (Cambridge Isotope Laboratories, Andover, MA). It was crystallized from isopropanol and packed (~0.5 mg of peptide) in a 1.3mm Bruker rotor together with crystalline KBr.

**Preparation of [U-^{13}C,^{15}N]-GB1**—E. coli BL21 (DE3) cells (Invitrogen) were transformed with the T2Q mutant of GB1. Cells were grown in M9 minimal media with 3.0 g of [U-^{13}C] glucose as the sole carbon source, and 1.0 g ^{15}N ammonium chloride as the sole nitrogen source (Cambridge Isotope Laboratories, Andover, MA). Protein expression was induced with 500 μM IPTG for 4 h. The cell pellet was homogenized with a tip sonicator in phosphate buffered saline (150 mM NaCl, 50 mM $KH_2PO_4$/$K_2HPO_4$, pH 7), and the supernatant purified by heating to 80 °C for 5 minutes followed by gel exclusion chromatography (Sephadex 16/60 Hi Prep). Peak purified fractions were pooled and concentrated using Amicon Ultra-3, 500 MWCO devices. Microcrystalline samples were

prepared according to ref. 45 by extensive dialysis in a total of 12L of 50 mM sodium phosphate buffer (pH 5.6) and precipitated with 3 aliquots of 2:1 MPD:IPA at a protein concentration of 25 mg/mL. The sample consisting of ~2.5 mg of protein was centrifuged into a 1.3 mm Bruker rotor.

**NMR Spectroscopy**—Experiments were performed on a commercial Bruker spectrometer operating at 500 MHz using a two channel $^1$H-$^{13}$C probe equipped with a 1.3 mm rotor/stator system. The spinning frequency was regulated with a Bruker MAS controller to $\pm$ 10 Hz.

### a. Microcrystalline [U-$^{13}$C,$^{15}$N]-MLF-OH

Experiments on the tripeptide utilized a 1.2 ms $^1$H-$^{13}$C CP contact time with 98 kHz $^{13}$C irradiation and the $^1$H rf field was ramped down through the n=1 Hartmann-Hahn condition (i.e. 163 kHz). Since MLF-OH is a dry peptide for which rf induced heating is less of an issue high power XiX decoupling ($\omega_1/2\pi$ =230 kHz) was employed during the $t_1$ and $t_2$ evolution periods with the optimal length of the XiX pulse was 60.2 $\mu$s (3.91 $\tau_r$). The spectral width in the direct and indirect dimension was 25.2 kHz. For the spectrum presented in Fig. SI7 the acquisition times were 27.7 ms in $t_2$ and 5 ms in $t_1$ with 8 scans per $t_1$ point (resulting in ~52 minute 2D experiment). For the spectra presented in Fig. SI4 the acquisition times were 27.7 ms in $t_2$ and 12.7 ms in $t_1$ with 64 scans per $t_1$ point (resulting in 17 h per 2D experiment). The recycle delay was 1.5 s. The temperature was maintained at 284 K (at the thermocouple) using a BCU-X with 1400 L/h nitrogen flow rate.

### b. Microcrystalline [U-$^{13}$C,$^{15}$N]-G$_{B1}$

The $^1$H-$^{13}$C CP contact time was 2.2 ms with 98 kHz $^{13}$C irradiation and $^1$H power ramped down through n=1 Hartmann-Hahn condition (i.e. 163 kHz). In order to minimize the rf induced heating of the hydrated protein sample we employed low power TPPM during both the direct and indirect evolution periods. Each pulse length was set to 30.77$\mu$s (corresponding to a modulation frequency $\omega_C/2\pi$ equal to a quarter of the MAS spinning frequency, i.e. 16.25 kHz) and the $^1$H decoupling was optimized by varying the $^1$H irradiation strength $\omega_{1H}/2\pi$ (near 16.25 kHz) and the phase excursion. The optimal phase excursion was $\pm24°$. The sweep width in the direct and indirect dimension was again 25.2 kHz. Acquisition times were 25 ms in $t_2$ and 10.1 ms in $t_1$ with 96 scans per $t_1$ point for the 2.5 ms spectrum (total acquisition time ~48 h) and 192 scan per $t_1$ point for the 10.1 ms spectrum (total acquisition time ~95.6 h). The recycle delay was 3.5 s.

### c. Optimization of PAR magnetization transfer

There are at least two methods that can be used to optimize the r.f. field strengths to satisfy the matching conditions for PAR experiments. The first relies on polarization transfer following a selective excitation pulse, and the second a comparison between the polarization transfer maps and "interference" maps. In either case we recommend that these maps be generated for the spinning frequencies of interest, and, accordingly, we have included a SPINEVOLUTION [46] script in the Supporting Information for this purpose. For reference Figure 2, Figure SI1, and Figure SI2 of this paper illustrate simulations corresponding to polarization transfer maps, and SI5 a interference maps for a simple model spin systems at $\omega_r/2\pi$ = 65 kHz. In our previous paper we published similar maps for $\omega_r/2\pi$ = 20 kHz [23].

In the first approach, which is commonly used for optimization of any ZQ sequence, we excite magnetization on one of the sites (C=O or C$\alpha$) using a selective pulse or selective CP together with a storage pulse followed by polarization transfer to a second site (e.g. C$\beta$'s), and the intensity of that signal is observed as a function of $^1$H and $^{13}$C field strengths. In order to constrain the search-space we employ a PAR polarization transfer map as is shown

in Figure 2 below as a guide. For the case illustrated in Figure 2, the map was calculated for polarization transfer from Cα to Cβ at $\omega_r/2\pi$ = 65 kHz, and indicates appreciable PAR transfer for $p_C$~1.12 or 1.75 (corresponding to $\omega_{1C}/2\pi$ = 72.8 kHz or 110.5 kHz) and $p_H$~0.3 or 1.3 (corresponding to $\omega_{1H}/2\pi$ = 19.5 kHz or 84.5 kHz), respectively. Using these parameters as a guide, we set the PAR mixing time to 2–3 ms (a period appropriate for transfer over short distances), the [13]C r.f field to 72.8 kHz, and we scan the [1]H r.f. field (e.g. from 10 to 40 kHz) looking for optimal transfer. In general we find it essential to perform such an optimization to account for omnipresent experimental variability. For example, depending on the probe, spectrometer, etc. the powers calibrated from 180º pulses may differ as much as 10 kHz from actual nutation frequencies. Thus, it is essential to accurately calibrate the [13]C r.f. field to use this method.

In the second approach we rely on a two step comparison between the PAR polarization transfer map and the interference map for choosing the appropriate r.f. settings. For example, in order to find the settings for a given $\omega_r/2\pi$, (say 20 kHz) we start with an experiment consisting of CP followed by 2–3 ms of PAR mixing with a relatively large ^{1}H field -- for instance, 83 kHz or another value that is sufficiently large to avoid Hartmann-Hahn conditions between ^{1}H and [13]C. We then observe the ^{13}C signal as the ^{13}C field strength is scanned from 15 to 50 kHz. During the scan we observe dips in ^{13}C signal when the r.f. field matches $\omega_r/2\pi$ and $2\omega_r/2\pi$ (i.e. 20 kHz and 40 kHz) due to the CSA recoupling at the rotary resonance recoupling ($R^3$) conditions at $p_C$= 1 or 2 [47], thus calibrating the ^{13}C power levels. Similarly, we can use Hartmann-Hahn matching to calibrate the ^{1}H power relative to the ^{13}C power. In particular, we fix the "calibrated" [13]C field strength at a value that leads to appreciable transfer in the PAR polarization transfer map, and then observe the ^{13}C signal as a function of the scan of the ^{1}H field strength. Referring to the polarization transfer map in Figure 2 of De Paepe, et. al. [23] which was calculated for $\omega_r/2\pi$ = 20 kHz, we set $\omega_{1C}/2\pi$ = 52 kHz and scan the ^{1}H irradiation from 5 kHz to 95 kHz. We observe dips in the ^{13}C signal for all the Hartmann-Hahn conditions i.e. $(\omega_{1H} \pm n\omega_r)/2\pi$ [explicitly at 52 ± (n x 20) kHz)]. From the $\omega_r/2\pi$ = 20 kHz PAR map we see that in order to achieve appreciable transfer for $p_C$ ~2.6 ($\omega_{1C}/2\pi$ = 52 kHz) we require ^{1}H fields with a strength slightly smaller that ^{13}C field ($p_H$ ~ 2.4 -- $\omega_{1H}/2\pi$ = 2.4*20 = 48 kHz). This can easily determined relative to the n=0 Hartmann-Hahn condition in our optimization (i.e. the dip in the ^{13}C signal for $\omega_{1H}/2\pi$ = 52 kHz). All of the experiments discussed here used this procedure, rather than the first method discussed above, for adjustment of the field strengths.

## Results and Discussion

Figure 1 depicts the pulse sequence used for recording 2D [13]C-^{13}C correlation spectra with the PAR mixing sequence which consists of the application of two CW fields. The irradiation strengths on the ^{1}H and ^{13}C channels are adjusted appropriately to induce polarization transfer between ^{13}C sites via the second order [13]C-[^{1}H]-^{13}C TSAR mechanism.[20,23] The PAR experiment is analyzed with average Hamiltonian theory (AHT) in detail elsewhere (ref. 23). Here we outline a few of the basic steps that lead to the expressions necessary for understanding the polarization transfer process.

We consider a three spin system consisting of two dipolar coupled [13]C's - [13]C $_1$, [13]C$_2$ - and an assisting ^{1}H spin subject to two CW rf fields of strength $\omega_{1C}$ and $\omega_{1H}$ applied to the ^{13}C and ^{1}H spins, respectively. The internal Hamiltonian can be written as

$$H = \omega_{C_1 H} 2 T_{10}^{C_1} T_{10}^{H} + \omega_{HC_2} 2 T_{10}^{H} T_{10}^{C_2} + \sqrt{6}\,\omega_{C_1 C_2} T_{20}^{C_1 C_2}$$
$$+ \Delta\omega_{C_1} T_{10}^{C_1} + \Delta\omega_{C_2} T_{10}^{C_2} + \Delta\omega_H T_{10}^{H}$$
$$+ \omega_{1C}\left\{ \frac{-T_{11}^{C_1} + T_{1-1}^{C_1}}{\sqrt{2}} \right\} + \omega_{1C}\left\{ \frac{-T_{11}^{C_2} + T_{1-1}^{C_2}}{\sqrt{2}} \right\} + \omega_{1H}\left\{ \frac{-T_{11}^{H} + T_{1-1}^{H}}{\sqrt{2}} \right\} \tag{1}$$

where $\Delta\omega_{C1}$, $\Delta\omega_{c2}$ and $\Delta\omega_H$ denote the shift tensors and resonant offsets of the $^{13}C$ (or $^{15}N$) and $^1H$ nuclei, respectively, and $\omega_{c1c2}$, $\omega_{C1H}$, and $\omega_{HC2}$ the homonuclear and heteronuclear dipolar couplings. For simplicity, we reduce the dependence on three different averaging frequencies [$\omega_r/2\pi$, the rotor frequency, and $\omega_{ic}/2\pi$ and $\omega_{1H}/2\pi$ the strength of the $^{13}C$ and $^1H$ CW fields, respectively] to a single frequency dependence by assuming that these frequencies are commensurate, implying that we can find indices $p_C$ and $p_H$, and integers $p_c^1, p_c^2, p_H^1, p_H^2$ such that

$$\omega_{1C}\big|_{2\pi} = p_C \left( \omega_r\big|_{2\pi} \right) = \frac{p_C^1}{p_C^2}\left( \omega_r\big|_{2\pi} \right) \tag{2}$$

$$\omega_{1H}\big|_{2\pi} = p_H \left( \omega_r\big|_{2\pi} \right) = \frac{p_H^1}{p_H^2}\left( \omega_r\big|_{2\pi} \right) \tag{3}$$

where $\dfrac{p_C^1}{p_C^2}, \dfrac{p_H^1}{p_H^2}$ denote irreducible ratios. The expression for the Hamiltonian in the interaction frame can thus be obtained from Eq. (1)

$$\tilde{H} = \overbrace{\sum_{m_1=-2} \sum_{\substack{q_{1C}=-1 \\ q_{1C}\neq 0}}^{1} \sum_{\substack{q_{1H}=-1 \\ q_{1H}\neq 0}}^{1} \omega_{C_1 H}^{m_1} \operatorname{sgn}(q_{1C})\operatorname{sgn}(q_{1H}) T_{1q_{1C}}^{C_1} T_{1q_{1H}}^{H} \exp\left\{ -i(nX_1)\frac{\omega_r t}{n} \right\}}^{1}$$

$$+ \overbrace{\sum_{m_2=-2} \sum_{\substack{q_{2C}=-1 \\ q_{2C}\neq 0}}^{1} \sum_{\substack{q_{2H}=-1 \\ q_{2H}\neq 0}}^{1} \omega_{HC_2}^{m_2} \operatorname{sgn}(q_{2H})\operatorname{sgn}(q_{2C}) T_{1q_{2H}}^{H} T_{1q_{2C}}^{C_2} \exp\left\{ -i(nX_2)\frac{\omega_r t}{n} \right\}}^{2}$$

$$+ \overbrace{\sum_{m_3=-2} \sum_{q_{3C}=-2}^{2} \omega_{C_1 C_2}^{m_3} d_{q_{3C}0}^{2}\left( -\pi\big|_2 \right) T_{2q_{3C}}^{C_1 C_2} \exp\left\{ -i(nX_3)\frac{\omega_r t}{n} \right\}}^{3} \tag{4}$$

$$+ \overbrace{\sum_{i=1}^{2} \sum_{m_i=-2} \sum_{\substack{q_{Ci}=-1 \\ q_{Ci}\neq 0}}^{1} \omega_{C_i}^{m_i}\left( \operatorname{sgn}(q_{C_i})/\sqrt{2} \right) T_{1q_{Ci}}^{C_i} \exp\left\{ -i(nX_{C_i})\frac{\omega_r t}{n} \right\}}^{4}$$

$$+ \overbrace{\sum_{m=-2} \sum_{\substack{q_H=-1 \\ q_H\neq 0}}^{1} \omega_H^{m}\left( \operatorname{sgn}(q_H)/\sqrt{2} \right) T_{1q_H}^{H} \exp\left\{ -i(nX_H)\frac{\omega_r t}{n} \right\}}^{5}$$

where we use the following expressions

$$X_1 = m_1 + p_C q_{1C} + p_H q_{1H}$$
$$X_2 = m_2 + p_H q_{2H} + p_C q_{2C}$$
$$X_3 = m_3 + p_C q_{3C} \qquad (5)$$
$$X_{Ci} = m_{Ci} + p_C q_{Ci}$$
$$X_H = m + p_H q_H$$

and sgn($q$) is the sign function of $q$.

We assume that the rf fields are chosen so that neither Hartmann-Hahn (H-H)[48] nor rotary resonance recoupling (R$^3$)[47] conditions are matched, i.e. $X_1 \neq 0, X_2 \neq 0, X_{Ci} \neq 0, X_H \neq 0$ and that the $^{13}$C-$^{13}$C dipolar coupling is not recoupled to first order ($X_3 \neq 0$). Under these conditions, the first order average Hamiltonian vanishes.

In order to describe the TSAR recoupling mechanism, we calculate the cross-term between terms 1 and 2 in Eq. (4)

$$\overline{H}_{1x2}^{(2)} = \sum_{\substack{m_1, q_{1C}, q_{1H}, \\ m_2, q_{2C}, q_{2H}}} \left[ \begin{array}{l} \frac{1}{2iT} \omega_{C_1 H}^{m_1} \mathrm{sgn}(q_{1C}) \mathrm{sgn}(q_{1H}) \, \omega_{HC_2}^{m_2} \, \mathrm{sgn}(q_{2H}) \, sg(q_{2C}) T_{1q_{1C}}^{C_1} T_{1q_{2C}}^{C_2} \left[ T_{1q_{1H}}^{H}, T_{1q_{2H}}^{H} \right] \\ \int_0^T dt_2 \int_0^{t_2} dt_1 \, (\exp\{-i\omega_r (X_1 t_2 + X_2 t_1)\} \exp\{-i\omega_r (X_2 t_2 + X_1 t_1)\}) \end{array} \right] \qquad (6)$$

One of the most important solutions of Eq. (6) is obtained for for $q_{1c} = -q_{2C}$ and $m_1 = -m_2$ which yields ZQ terms of the form $T_{1m}^{C_1} T_{1\pm 1}^{C_2} T_{10}^{H}$ (also providing that we concurrently avoid the DQ conditions associated with $p_C = \{0, \pm 0.5, \pm 1, \pm 1.5, \pm 2\}$, H-H conditions with $p_C = \pm p_H \pm \{1, 2\}$, and R$^3$ conditions with $p_C = \{1, 2\}$). With these constraints we obtain the following expression for the second order TSAR term:

$$\begin{aligned} \overline{H}_{1x2}^{(2)} &= 2\omega_{TSAR} \left( T_{11}^{C_1} T_{1-1}^{C_2} \right) T_{10}^{H} + 2\omega_{TSAR}^* \left( T_{1-1}^{C_1} T_{11}^{C_2} \right) T_{10}^{H} \\ &= 2\omega_{TSAR} C_1^+ C_2^- H_z + 2\omega_{TSAR}^* C_1^- C_2^+ H_z \qquad (7) \\ &= \mathrm{Re}\,(\omega_{TSAR}) 2I_{C_1 C_2, X}^{(23)} I_{H,z} + \mathrm{Im}\,(\omega_{TSAR}) 2I_{C_1 C_2, Y}^{(23)} I_{H,z} \end{aligned}$$

and the TSAR coupling:

$$\omega_{TSAR} = \left( \frac{\mathrm{Re}\left(\omega_{C_1 H}^1 \, \omega_{HC_2}^{-1}\right)}{\omega_r} \lambda(1, p_C, p_H) + \frac{\mathrm{Re}\left(\omega_{C_1 H}^2 \, \omega_{HC_2}^{-2}\right)}{\omega_r} \lambda(2, p_C, p_H) \right)$$
$$+ i\left( \frac{\mathrm{Im}\left(\omega_{C_1 H}^1 \, \omega_{HC_2}^{-1}\right)}{\omega_r} \sigma(1, p_C, p_H) + \frac{\mathrm{Im}\left(\omega_{C_1 H}^2 \, \omega_{HC_2}^{-2}\right)}{\omega_r} \sigma(2, p_C, p_H) \right) \qquad (8)$$

with

$$\lambda(m, p_C, p_H) = \left( \frac{-(p_C + p_H)}{m^2 - (p_C + p_H)^2} + \frac{-(p_H - p_C)}{m^2 - (p_H - p_C)^2} \right)$$
$$\sigma(m, p_C, p_H) = \left( \frac{m}{m^2 - (p_H + p_C)^2} - \frac{m}{m^2 - (p_H - p_C)^2} \right) \qquad (9)$$

The above expressions permit us to visualize the subspace in which the TSAR spin dynamics evolve. The TSAR subspace (Fig. SI6) can be viewed as a coupled basis described extensively in the context of solution NMR between a fictitious ZQ operator involving the two $^{13}$C's and a $^1$H. The proton spin is essentially a bystander spin i.e. no magnetization is

sent to this proton in the spin dynamics described by Eq. (7). In this process, the dipolar couplings to the $^1$H are used to create an effective transverse PAR component composed of trilinear terms of the form $C_1^{\pm} C_2^{\mp} H_z$ that mediates polarization transfer. Another important contribution to the spin dynamics in the TSAR mechanism arises from auto-cross terms created by term 1 with itself and term 2 with itself respectively. These auto-cross terms lead to an off-resonance contribution in the TSAR subspace represented by $I_{C_1 C_2, Z}^{(23)}$. Note that similar longitudinal terms also arise from the chemical shift tensor with itself. Such contributions lead to a tilting of the effective recoupling axis and reduction of the PAR polarization transfer.

Figure 2 shows a numerical SPINEVOLUTION[46] simulation of the $^{13}$C-$^{13}$C PAR polarization transfer at $\omega_r/2\pi = 65$ kHz on a 7 spin system consisting of four $^{13}$C's and three $^1$H's (see the inset of the Fig. 2 and Table SI1 for details). The contour plot illustrates the transfer from $C_\alpha$ to $C_\beta$ (see Fig. SI1 for $C_\alpha$-C' and $C_\alpha$-$C_\beta$ optimization maps) after 5 ms of PAR mixing as a function of $^{13}$C and $^1$H C.W. irradiation amplitudes in units of spinning frequency ($p_C = \omega_{1C}/\omega_r$ and $p_H = \omega_{1H}/\omega_r$ respectively). The carrier frequency in the simulation was set between the carbonyl and aliphatic resonances, similar to the actual experiments (see Fig. SI2 for an optimization map with the $^{13}$C carrier frequency set in the middle of the aliphatic region only). There are several areas in the map for which the settings lead to appreciable PAR polarization transfer. The settings employed in this study are indicated with an '**X**', including the higher power settings used for the $^{13}$C-$^{13}$C correlation spectra of N-*f*MLF-OH[26] (see Fig. 5 and Fig. SI4) and lower power settings used for the correlation spectra of GB1.

The PAR optimization map arises from a compromise between maximizing the TSAR term and minimizing the longitudinal contribution from the auto-cross terms. The experimental irradiation settings were chosen as described in ref. 23. More specifically, we have simulated a map where we monitor $^{13}$C magnetization as a function of $^1$H and $^{13}$C irradiation in a 1D experiment with 5 ms PAR mixing. Such an "interference" map (also simulated numerically in Fig. SI5) permits identification of the rf fields that lead to destructive interference and it also outlines the features of the PAR polarization transfer map. Comparing the interference maps (both simulation and experiment) and the polarization transfer map shown in Fig. 2 allows one to choose the appropriate rf settings. Note, that for both the N-*f*MLF-OH and GB1 spectra presented below, we have chosen settings that favor polarization transfer between protonated $^{13}$C's but also allow transfer between carbonyls and aliphatic $^{13}$C's (with slightly lower efficiency). If the goal of the experiment is to maximize the magnetization transfer between carbonyls and protonated $^{13}$C's, the reader should refer to Fig. SI1b to choose the appropriate rf power levels. The shift in rf settings can be explained by the variation in magnitude of the auto-cross terms involved in a PAR carbonyl to aliphatic versus PAR aliphatic to aliphatic transfer.

Combining >50 kHz spinning frequencies and low power $^1$H decoupling was shown previously to yield very well resolved spectra in uniformly labeled proteins.[40] The concept of low power decoupling (introduced by Ernst *et al.*) was also investigated at $\omega_r/2\pi \sim 30$ kHz by De Paëpe *et al.* in the context of the Cosine Modulation[18,51] and Two Pulse Phase Modulation[52] irradiation scheme where an rf field strength close to the $\omega_r/4$ and a phase angle ~20 degrees was shown to yield efficient decoupling settings.[49] This sequence was recently discussed in greater detail by Kotecha *et al.* at ~40 kHz spinning frequency and referred to as low power TPPM.[50] Figure 3 shows CP-MAS spectra obtained on microcrystalline [U-$^{13}$C,$^{15}$N] protein GB1 recorded at $\omega_{H0}$=500 MHz, $\omega_r/2\pi$=65 kHz with low power TPPM[49,50] (~ $\omega_{1C}$=$\omega_r/4$=16.25 kHz, $\varphi$=±24°) during the acquisition. Although

this system has already been demonstrated to yield well resolved spectra in previous publications, it is worthwhile to point out the excellent resolution achieved in this experiment. Notably, we observe well resolved aromatic carbon resonances which appear more intense than in any SSNMR study on GB1 reported so far.[53,54] Moreover we also observe splittings due to J-coupling for most of the sites in the protein.

Several factors could contribute to the excellent resolution of the $\omega/2\pi = 65$ kHz MAS spectra reported here, including very effective heteronuclear decoupling, efficient averaging of the residual anisotropic contributions (i.e. magnetic bulk susceptibility etc.), and reduction of thermal gradients across the sample compared to a larger rotor[††]. This result clearly indicates that low power decoupling methods at $\omega_r/2\pi > 50$ kHz provide a viable method for carrying out high resolution protein studies.

Figure 4 shows a 2D $^{13}C$-$^{13}C$ PAR spectrum of microcrystalline [U-$^{13}C$,$^{15}N$] protein GB1 at $\omega_r/2\pi = 65$ kHz, $\omega_{0H}/2\pi = 500$ MHz where low power TPPM[49,50] $^1H$ decoupling ($\omega_{1H}/2\pi \sim 0.25\ \omega_r/2\pi = 16.25$ kHz) was applied during both direct and indirect evolution. 10 ms PAR mixing was used with the irradiation settings corresponding to the black cross noted '**X**' on Fig. 2. The spectrum shows cross peaks corresponding to both intra-residue and inter-residue medium to long distance contacts. Some representative long distance cross peaks are marked on the PAR spectrum (Fig. 4) and the corresponding contacts are shown on the rendering of the x-ray structure[45] with the distances indicated in Fig. 4c.

This result demonstrates that long distance transfers can be observed even at $\omega/2\pi = 65$ kHz with only 10 ms PAR mixing. This mixing time falls approximately in the same range as those used at $\omega/2\pi = 20$ kHz to perform the *de novo* structure determination of the protein Crh and thus implies that similar work is feasible at > 50 kHz spinning frequencies.[22,23] To complement Fig. 4, a shorter PAR mixing time (2.5 ms) containing primarily one-bond and two-bond cross-peaks can be found in Fig. SI3.

Since the TSAR mechanism is based on a second order process it is not completely intuitive that the PAR mixing time required for observing a given distance transfer does not increase as the spinning frequency increases. However, as discussed in De Paepe, et. al. 23 the higher MAS rates allow one to choose rf settings with an improved scaling factor that can compensate for lower transfer efficiencies. This feature is essential to allow practical implementations of PAR experiments at $\omega/2\pi > 30$ kHz and contrasts with PDSD[56] and DARR[15,17] which would require orders of magnitude longer mixing times. Note that in a recent study by Scholz et al. already at much lower spinning frequency of 45 kHz could not observe appreciable one-bond polarization transfer using conventional PDSD or n=1,2 DARR.[43]

The excellent resolution achieved with low power TPPM decoupling at $\omega_r/2\pi = 65$ kHz is already obvious from the 1D spectrum displayed in Fig. 3, but is further illustrated in the 2D $^{13}C$-$^{13}C$ PAR spectrum. The inset in Fig. 4 shows expansions of selected carbonyl-aliphatic cross peaks from the spectra processed without (Fig. 4a) and with linear prediction in the direct dimension (Fig. 4b). We can clearly distinguish J-splittings for most of the resonances in the spectrum.

The mixing period and decoupling settings used for the PAR experiment on protein GB1 were chosen to optimize resolution and sensitivity while minimizing rf power requirements and thus rf induced sample heating. However, for samples where rf induced heating is less

---

[††]According to Doty et al. the thermal gradient due to the rf heating in a solenoid coil is proportional at least to the 4th power of the rotor diameter. (55) Doty, F. D.; Kulkarni, J.; Turner, C.; Entzminger, G.; Bielecki, A. J Magn Reson 2006, 182, 239.

of a concern, higher power settings for both the PAR mixing and the ^{1}H decoupling periods can be used. As an illustration Fig. SI4 shows $^{13}$C-$^{13}$C PAR spectra obtained on the dry, crystalline tripeptide [U-$^{13}$C,$^{15}$N]-*f*-MLF-OH with high power PAR mixing (the settings are indicated with a blue cross noted "**X**" in Fig. 2) and with ~230 kHz XiX[57,58] decoupling during both direct and indirect evolution periods. Note that in these data we observe clear cross-peaks between the carbons in the phenylalanine ring, which undergoes two-fold flipping motion in the temperature regimes employed for most MAS experiments.

In summary we demonstrate that the $^{13}$C-$^{13}$C PAR method can be used to obtain long distance $^{13}$C-$^{13}$C contacts in uniformly $^{13}$C labeled proteins at $\omega_r/2\pi = 65$ kHz with mixing times of ~10 ms or less. Moreover, the PAR irradiation settings can be chosen to minimize rf induced heating even at such high spinning frequencies. This application opens up a venue for *de novo* structure determination of proteins at $\omega_r/2\pi > 50$ kHz in a manner analogous to the studies performed at lower spinning frequencies. Notably, PAR provides a flexible tool for structural characterization of biomolecules over the entire range of currently available spinning frequencies and can be used alone or as a building block in more sophisticated pulse sequences.

We also demonstrate that combination of >50 kHz spinning frequency and low power decoupling provides an attractive method for carrying out high resolution protein studies by solid-state NMR. The resolution of the spectra obtained at $\omega_r/2\pi=65$ kHz with low power TPPM rivals or surpasses the resolution obtainable at $\omega_r/2\pi < 30$ kHz with high power decoupling, but with significantly reduced rf strength requirements.

## Supplementary Material

Refer to Web version on PubMed Central for supplementary material.

## Acknowledgments

## Biographies



*Józef R. Lewandowski* received his B.A. in Chemistry and Theater & Dance from Amherst College (2002) and his Ph.D. in Chemistry from MIT (2008). He is currently a Marie Curie Postdoctoral Fellow at the Ecole Normale Supérieure de Lyon in France. His research is focused on the application and development of solid-state NMR methodology for protein dynamics and structure determination

**Gaël De Paëpe** received his B.S. and his Ph.D. in Physics from the Ecole Normale Supérieure de Lyon (2004). After spending four years as an postdoctoral pesearcher at the Massachusetts Institute of Technology, he joined the Grenoble Institute for Nanoscience and Cryogenics in 2008, where he currently holds an ANR Chair of Excellence. His research is focused on developing new methods for structure determination by solid-state NMR as well as new instrumentation and methods for high field dynamic nuclear polarization (DNP).



*Matthew T. Eddy* received his B.A. in Chemistry from Oberlin College (2004) and is currently a chemistry Ph.D. student in the laboratory of Prof. Robert G. Griffin at MIT. At Oberlin College, Matthew was first introduced to MAS NMR under the guidance of Professor Manish Mehta who inspired him to pursue further studies in the area. Matthew's research interests include the development of MAS NMR methodology and applications on ion channels and fibrillar proteins.



**Jochem O. Struppe** received his Diploma in Physics (1992) and his Dr. re. nat. degree in Physics (1996) from Technische Universität Stuttgart. After spending 2 years as postdoctoral researcher at UCSD in the department of Chemistry and Biochemistry, he joined Bruker BioSpin, where he is currently senior scientist in the applications department. He focuses on support and development of solid state NMR experimental techniques, development of NMR probes, solid state NMR with DNP and particularly solid state NMR with biological systems.



**Werner E. Maas** was an undergraduate and holds a Ph.D. (1992) from the University of Nijmegen in the Netherlands. He is currently Executive Vice President for Bruker BioSpin Corp. His interests lie in the development of magnetic resonance technology and its applications in the fields of chemistry, biochemistry, materials science and clinical diagnostics

**Robert G. Griffin** was an undergraduate at the University of Arkansas, graduating with a BS (honors) in Chemistry (1964). He received his Ph.D. from Washington University-St. Louis (1969) with S.I. Weissman working on electron spin resonance of radical ions. He was a postdoctoral fellow (1970–72) with J.S. Waugh at MIT in the early days of high resolution solid state NMR. In 1972 he became a staff member at the Francis Bitter Magnet Laboratory where he is currently Director. In 1989 he became Professor of Chemistry at MIT. In 2007 Prof. Griffin received the Laukien Prize of the Experimental NMR Conference and the Eastern Analytical Society Award for outstanding contributions to magnetic resonance.

## References

1. Andrew ER, Bradbury A, Eades RG. Nature. 1959; 183:1802.
2. Lowe IJ. Phys. Rev. Letters. 1959; 2:285.
3. Griffin RG. Nature Structural Biology. 1998; 5:508.
4. Raleigh DP, Levitt MH, Griffin RG. Chemical Physics Letters. 1988; 146:171.
5. Bennett AE, Ok JH, Griffin RG, Vega SJ. Chem. Phys. 1992; 96:8624.
6. Bennett AE, Rienstra CM, Griffiths JM, Zhen WG, Lansbury PT, Griffin RG. J. Chem. Phys. 1998; 108:9463.
7. Hohwy M, Nielsen NC. J. Chem. Phys. 1997; 106:7571.
8. Hohwy M, Rienstra CM, Jaroniec CP, Griffin RG. J. Chem. Phys. 1999; 110:7983.
9. Hohwy M, Rienstra CM, Griffin RG. J. Chem. Phys. 2002; 117:4973.
10. Rienstra CM, Hatcher ME, Mueller LJ, Sun BQ, Fesik SW, Griffin RG. J. Am. Chem. Soc. 1998; 120:10602.
11. Carravetta M, Eden M, Zhao X, Brinkmann A, Levitt MH. Chemical Physics Letters. 2000; 321:205.
12. Brinkmann A, Eden M, Levitt MH. J. Chem. Phys. 2000; 112:8539.
13. Jaroniec CP, Filip C, Griffin RG. J. Am. Chem. Soc. 2002; 124:10728. [PubMed: 12207528]
14. Brinkmann A, Levitt MH. J. Chem. Phys. 2001; 115:357.
15. Takegoshi K, Nakamura S, Terao T. Chemical Physics Letters. 2001; 344:631.
16. Verel R, Ernst M, Meier BH. J. Magn. Reson. 2001; 150:81. [PubMed: 11330986]
17. Takegoshi K, Nakamura S, Terao TJ. Chem. Phys. 2003; 118:2325.
18. De Paepe G, Elena B, Emsley LJ. Chem. Phys. 2004; 121:3165.
19. De Paepe G, Bayro MJ, Lewandowski J, Griffin RG. J Am Chem Soc. 2006; 128:1776. [PubMed: 16464061]
20. Lewandowski JR, De Paepe G, Griffin RG. J Am Chem Soc. 2007; 129:728. [PubMed: 17243786]
21. Tycko RJ. Chem. Phys. 2007:126.
22. De Paepe G, Lewandowski JR, Griffin RG. J Chem Phys. 2008; 128:124503. [PubMed: 18376939]
23. De Paepe G, Lewandowski J, Locquet A, Bockmann A, Griffin RG. J. Chem. Physics. 2008; 129:245101.
24. Creuzet F, McDermott A, Gebhard R, Vanderhoef K, Spijkerassink MB, Herzfeld J, Lugtenburg J, Levitt MH, Griffin RG. Science. 1991; 251:783. [PubMed: 1990439]
25. Griffiths JM, Lakshmi KV, Bennett AE, Raap J, Vanderwielen CM, Lugtenburg J, Herzfeld J, Griffin RG. J. Am. Chem. Soc. 1994; 116:10178.

26. Rienstra CM, Tucker-Kellogg L, Jaroniec CP, Hohwy M, Reif B, McMahon MT, Tidor B, Lozano-Perez T, Griffin RG. Proceedings of the National Academy of Sciences of the United States of America. 2002; 99:10260. [PubMed: 12149447]

27. Jaroniec CP, MacPhee CE, Bajaj VS, McMahon MT, Dobson CM, Griffin RG. Proceedings of the National Academy of Sciences of the United States of America. 2004; 101:711. [PubMed: 14715898]

28. Castellani F, van Rossum B, Diehl A, Schubert M, Rehbein K, Oschkinat H. Nature. 2002; 420:498.

29. Samoson A, Tuherm T, Gan Z. Solid State Nuclear Magnetic Resonance. 2001; 20:130. [PubMed: 11846236]

30. Samoson A, Tuherm T, Past J, Reinhold A, Anupold T, Heinmaa N. New horizons for magic-angle spinning NMR. New Techniques in Solid-State Nmr. 2005; Vol. 246:15.

31. Reif B, Jaroniec CP, Rienstra CM, Hohwy M, Griffin RG. J. Magn. Reson. 2001; 151:320. [PubMed: 11531354]

32. Reif B, Griffin RG. J. Magn. Resonance. 2003; 160:178.

33. Chevelkov V, Rehbein K, Anne Diehl, Reif B. Angew. Chem. Int. Ed. 2006; 45:3878.

34. Zhou DH, Shah G, Cormos M, Mullen C, Sandoz D, Rienstra CM. J. Am. Chem. Soc. 2007; 129:11791. [PubMed: 17725352]

35. Zhou DH, Shea JJ, Nieuwkoop AJ, Franks WT, Wylie BJ, Mullen C, Sandoz D, Rienstra CM. Angewandte Chemie-International Edition. 2007; 46:8380.

36. Bayro MJ, Ramachandran R, Caporini MA, Eddy MT, Griffin RG. J. Chem. Phys. 2008:128.

37. De Paepe G, Lewandowski J, Locquet A, Bockmann A, Griffin RG. preparation. 2008

38. Ernst M, Samoson A, Meier BH. Chemical Physics Letters. 2001; 348:293.

39. Ernst M, Detken A, Bockmann A, Meier BH. J. Am. Chem. Soc. 2003; 125:15807. [PubMed: 14677971]

40. Ernst M, Meier MA, Tuherm T, Samoson A, Meier BH. J. Am. Chem. Soc. 2004; 126:4764. [PubMed: 15080665]

41. Verel R, Baldus M, Ernst M, Meier BH. Chemical Physics Letters. 1998; 287:421.

42. Laage S, Sachleben J, Steuernagel S, Pierattelli R, Pintacuda G, Emsley L. Jour. Magn. Resonance. 2008 (in press).

43. Scholz I, Huber M, Manolikas T, Meier BH, Ernst M. Chemical Physics Letters. 2008; 460:278.

44. Lewandowski JR, De Paëpe G, Eddy MT, RG G. Jour. Am. Chem. Soc. 2009 (in press).

45. Franks WT, Zhou DH, Wylie BJ, Money BG, Graesser DT, Frericks HL, Sahota G, Rienstra CM. J. Am. Chem. Soc. 2005; 127:12291. [PubMed: 16131207]

46. Veshtort M, Griffin RG. J. Magn. Reson. 2006; 178:248. [PubMed: 16338152]

47. Oas TG, Griffin RG, Levitt MH. J. Chem. Phys. 1988; 89:692.

48. Hartmann SR, Hahn EL. Phys. Rev. 1962; 128:2042.

49. De Paepe G. Heteronuclear Decoupling in Solid State Nuclear Magnetic Resonance. Doctoral, École Normale Supèrieure de Lyon. 2004

50. Kotecha M, Wickramasinghe NP, Ishii Y. Magn Reson Chem. 2007; 45:S221.

51. De Paepe G, Hodgkinson P, Emsley L. Chemical Physics Letters. 2003; 376:259.

52. Bennett AE, Rienstra CM, Auger M, Lakshmi KV, Griffin RG. J. Chem. Phys. 1995; 103:6951.

53. Franks WT, Kloepper KD, Wylie BJ, Rienstra CM. J Biomol NMR. 2007; 39:107. [PubMed: 17687624]

54. Schmidt HLF, Sperling LJ, Gao YG, Wylie BJ, Boettcher JM, Wilson SR, Rienstra CA. Journal of Physical Chemistry B. 2007; 111:14362.

55. Doty FD, Kulkarni J, Turner C, Entzminger G, Bielecki A. J Magn Reson. 2006; 182:239. [PubMed: 16860580]

56. Szeverenyi NM, Sullivan MJ MacielGE. J. Magn. Reson. 1982; 47:462.

57. Tekely P, Palmas P, Canet D. Journal of Magnetic Resonance Series A. 1994; 107:129.

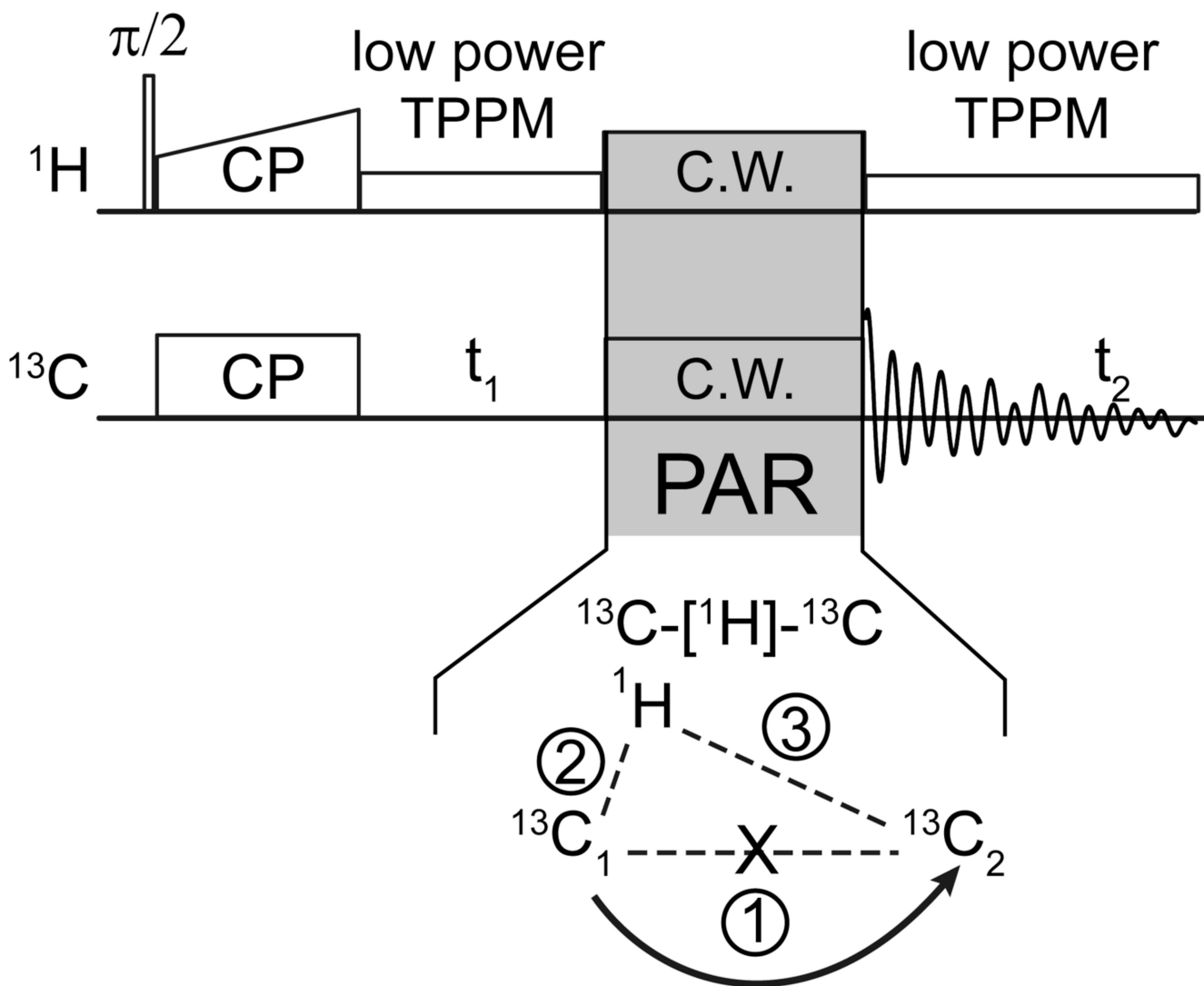58. Detken A, Hardy EH, Ernst M, Meier BH. Chemical Physics Letters. 2002; 356:298.

**Figure 1.**
Pulse sequence for 2D $^{13}C$-$^{13}C$ PAR experiments. The PAR mixing consists of simultaneous C.W. irradiation on the $^{1}H$ and $^{13}C$ channels with the irradiation strengths chosen to produce an appreciable second order TSAR mechanism.[20,23] The TSAR term is a result of a cross term between the $^{1}H$-$^{13}C$ dipolar couplings (terms 2 and 3 in the spin system figure).
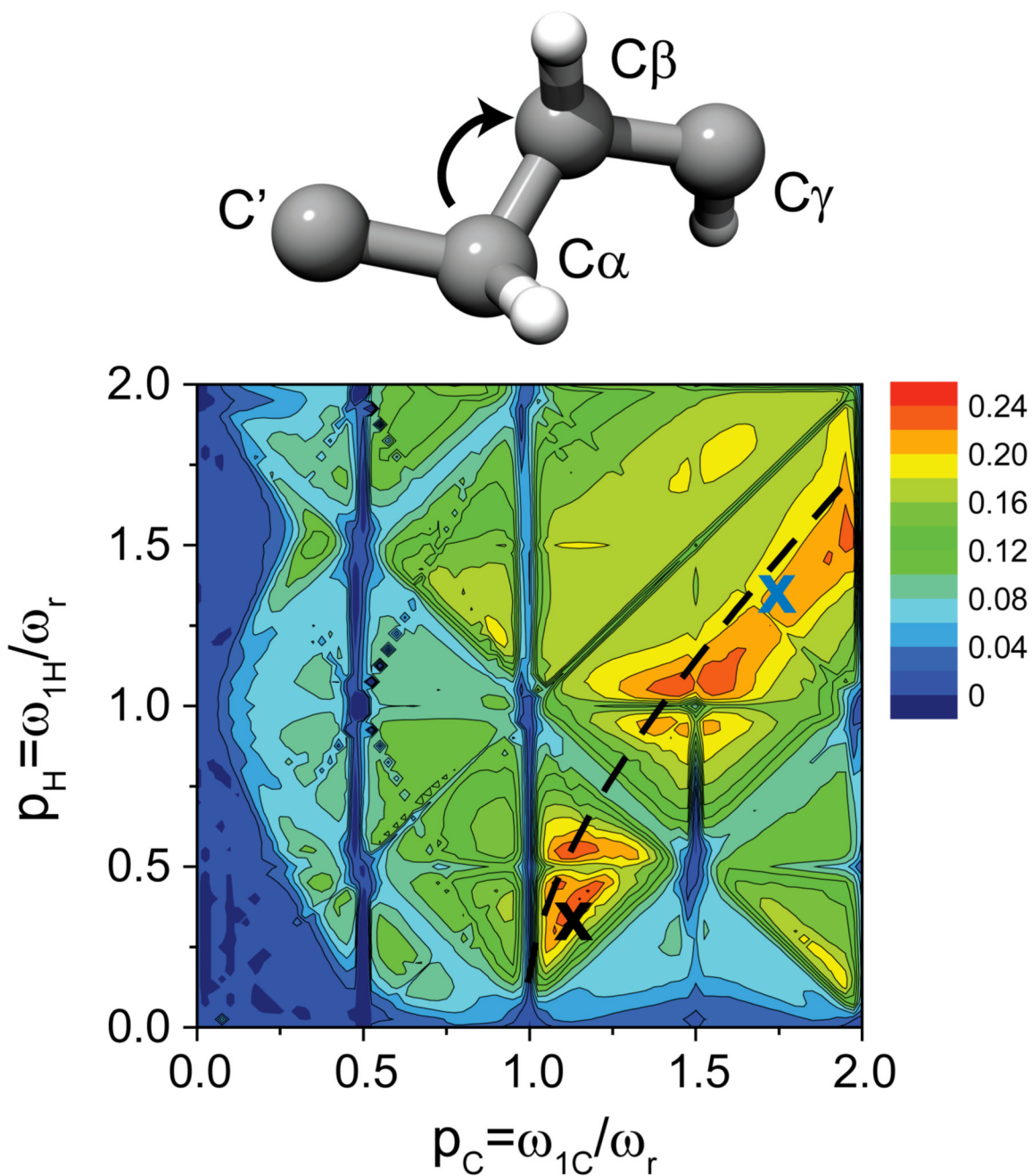
**Figure 2.**
Simulated PAR polarization transfer map obtained on the spin system shown in the inset of the figure (see also Table SI1). The contour plots represent polarization transfer between the $C_\alpha$ and $C_\beta$ spins as a function of $^{13}$C and $^{1}$H irradiation strengths in units of spinning frequency. Simulations were performed using 5 ms PAR mixing at $\omega_r/2\pi = 65$ kHz and $\omega_{0H}/\pi = 500$ MHz and include chemical shifts (see Table SI1). Similar maps for $C_\alpha$-C' and $C_\alpha$-$C_\beta$ polarization transfer can be found in Fig. SI1. For the settings indicated by the black dashed lines the CH auto-cross term is zero. The irradiation settings employed in this study are indicated with 'x's (blue for N-f-MLF-OH and black for GB1).
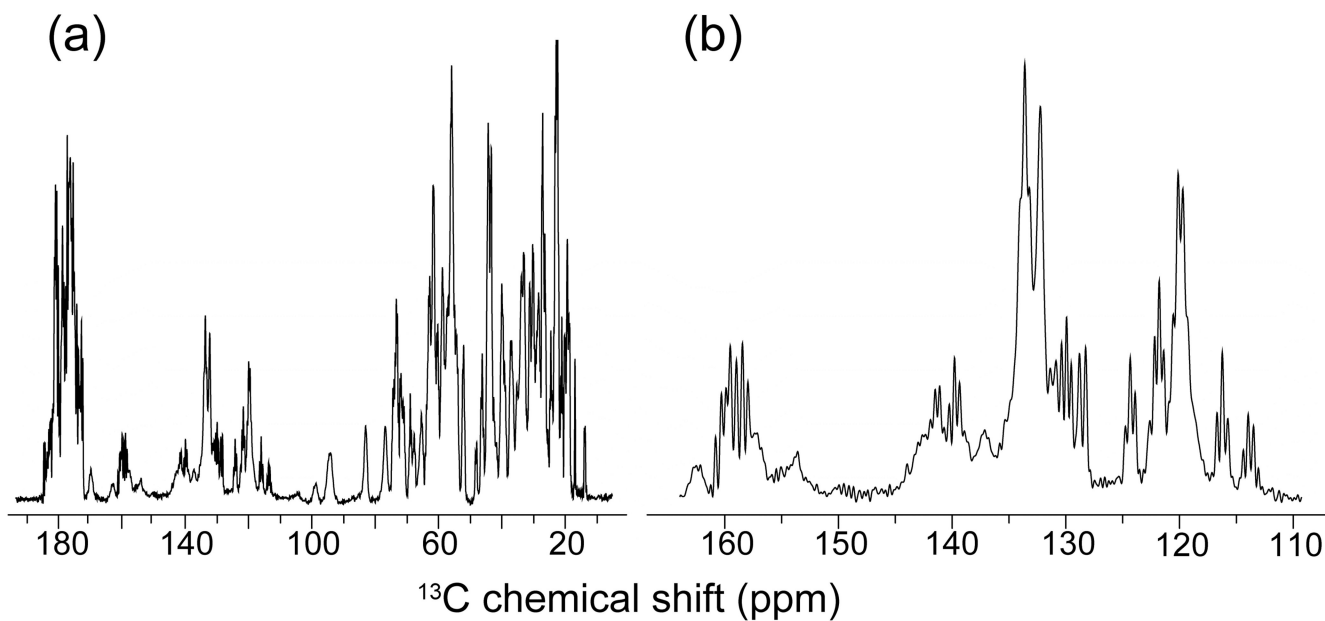
(a) (b)

$^{13}$C chemical shift (ppm)

**Figure 3.**
(a) 1D $^{13}$C CP-MAS spectrum of microcrystalline [U-$^{13}$C,$^{15}$N]-GB1 (2.5 mg protein packed in 1.3 mm rotor) obtained at $\omega_r/2\pi$ = 65 kHz and $\omega_{0H}/2\pi$ = 500 MHz with low power (~16.25 kHz) TPPM decoupling49,50 during acquisition. (b) Expansion of the aromatic region illustrating the excellent resolution.
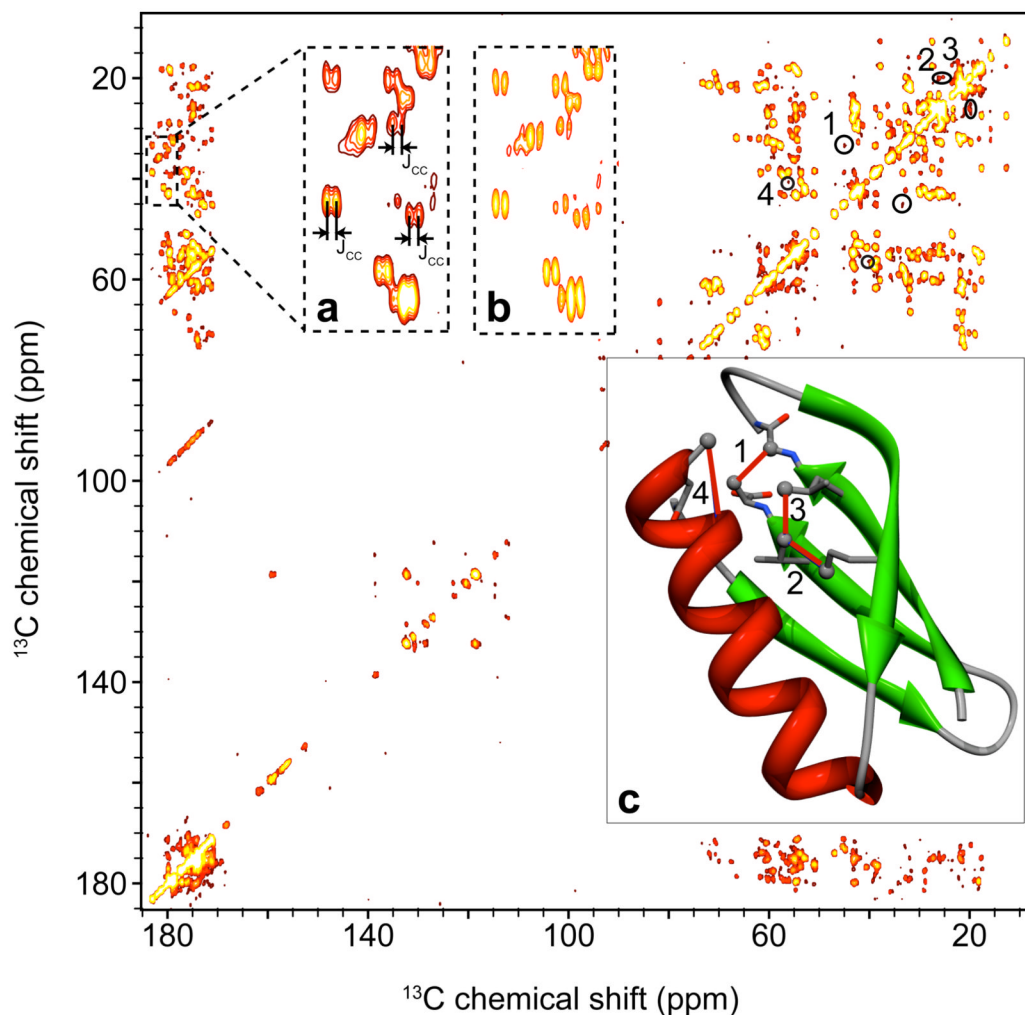
**Figure 4.**
2D $^{13}$C-$^{13}$C PAR correlation spectra of microcrystalline [U-$^{13}$C,$^{15}$N]-GB1 obtained at $\omega_r/2$ = 65 kHz and $\omega_{0H}/2$ = 500 MHz with 10 ms PAR mixing. The PAR mixing employed ~73 kHz $^{13}$C and 19.5 kHz $^{1}$H irradiation. Low power TPPM49,50 ($\omega_{1C}$= $\omega_r/4$=16.25 kHz) was applied during acquisition and $t_1$ evolution. The high resolution achievable with this decoupling scheme is illustrated in panels (a) and (b), which depict an expansion of a carbonyl-aliphatic region of the spectrum. The data in panel (a) were processed without linear prediction in the direct dimension ($t_2$=25 ms) and the data in panel (b) with liner prediction in the direct dimension. In both panels in the direct dimension we can clearly distinguish splitting due to the J-couplings for most of the cross-peaks. Panel (c) illustrates some of the representative long distance contacts that are observed in an experiment with 10 ms PAR mixing. The cross-peaks corresponding to the contacts in panel (c) are circled and marked with numbers in the spectrum: 1 - E56C$\beta$-G9C$\alpha$ – 4.1 Å, 2 – L7C$\delta$2-L5C$\gamma$2 – 4.0 Å, 3 – L7C$\delta$2-V54C$\gamma$1 – 3.8 Å, 4 – N37C$\beta$-A34C$\alpha$ – 4.8 Å.